The metal bonding domain of the antitumor drug Fe(II)-bleomycin: a DFT investigation

Karawajczyk, A.; Buda, F.

J Biol Inorg Chem (2005) 10: 33–40
DOI 10.1007/s00775-004-0610-8

ORIGINAL ARTICLE

Anna Karawajczyk · Francesco Buda

The metal bonding domain of the antitumor drug Fe(II)-bleomycin: a DFT investigation

Received: 21 July 2004 / Accepted: 21 October 2004 / Published online: 1 December 2004

Abstract The geometric and electronic structure of ferrous complexes of bleomycin (Fe(II)BLM) has been investigated by means of density functional theory (DFT) calculations. The active site of this antitumor drug is a highly distorted octahedral complex, with the coordination sphere completed by the five known endogenous ligands, including pyrimidine, imidazole, deprotonated amide, and secondary and primary amines. We have addressed the controversial issue of the nature of the sixth axial ligand, which we have identified as the oxygen of the carbamoyl group. Our conclusions are further validated by a comparison with structural data derived from NMR experiments. Moreover, because of the high sensitivity of structural data on the pH of the environment, we have investigated the effect of a different protonation state of the histidine amide on the geometric structure of the Fe(II)BLM complex. The extensive model of the active site of bleomycin considered in this work allows us to check the limitations of previous investigations based on simplified models.

Keywords Bleomycin · Density functional theory · Iron complex · Structural model

Abbreviations aALA: aminoalanine · ABLM: activated bleomycin · BITH: bithiazole · BLM: bleomycin · GUL: gulose · MAN: mannose · mVAL: methylovalerate · PYR: pyrimidinylpropionamide · RMSD: root mean square deviation · THR: threonine

Electronic Supplementary Material Supplementary material is available for this article if you access the article at http://dx.doi.org/10.1007/s00775-004-0610-8. A link in the frame on the left on that page takes you directly to the supplementary material.

A. Karawajczyk · F. Buda (✉)
Leiden Institute of Chemistry, Gorlaeus Laboratories,
2300 RA Leiden, The Netherlands
E-mail: f.buda@chem.leidenuniv.nl
Fax: +31-71-5274603

Introduction

Bleomycin (BLM) is a DNA-cleaving antibiotic isolated as a copper complex from the culture medium of *Streptomyces verticillis*, but administrated to patients in metal-free form. BLM is important for clinical use in the treatment of head and neck cancer, certain lymphomas, and testicular cancer [1]. Interest in the chemical activity of bleomycin began with the discovery that the presence of either reducing agents or hydrogen peroxide permits bleomycin to cleave DNA into simple sets of DNA degradation products [2]. Indications that metals and oxygen species were also required led to the demonstration that the presence of Fe(II) and O_2 was sufficient to allow BLM to degrade DNA. The first step is the formation of a high-spin Fe(II)BLM complex which reacts with O_2 [3]. In the second step, the so-called activated bleomycin (ABLM) – a peroxide-Fe(III)BLM complex – is produced and this then cleaves DNA. The products of DNA degradation are well known [2], but major gaps in our understanding remain where the drug activation and DNA degradation pathways intersect. A precise knowledge of the geometrical and electronic structure of the Fe(II)BLM complex is a prerequisite to understanding the activity of this drug in DNA degradation.

Unfortunately, no crystal structure is yet available for Fe(II)BLM. There are several different synthesized models mimicking BLM as a ligand and crystallized with various metals, for example copper [4, 5], cobalt [6], zinc [7], and even iron [8]. However, all of them lack both the bithiazole and the sugar residues. For example, the PMAH ligand (see Fig. 1) has five nitrogen donor centers located in the primary and secondary amines, pyrimidine and imidazole rings, and the amide moiety. The ligand synthesized for iron is only tridentate, since the β-aminoalanine fragment is also not present. Therefore these crystallographic studies could not give a definitive answer as to whether the bleomycin is a five- or six- coordinated ligand and, if the sixth ligand is in-

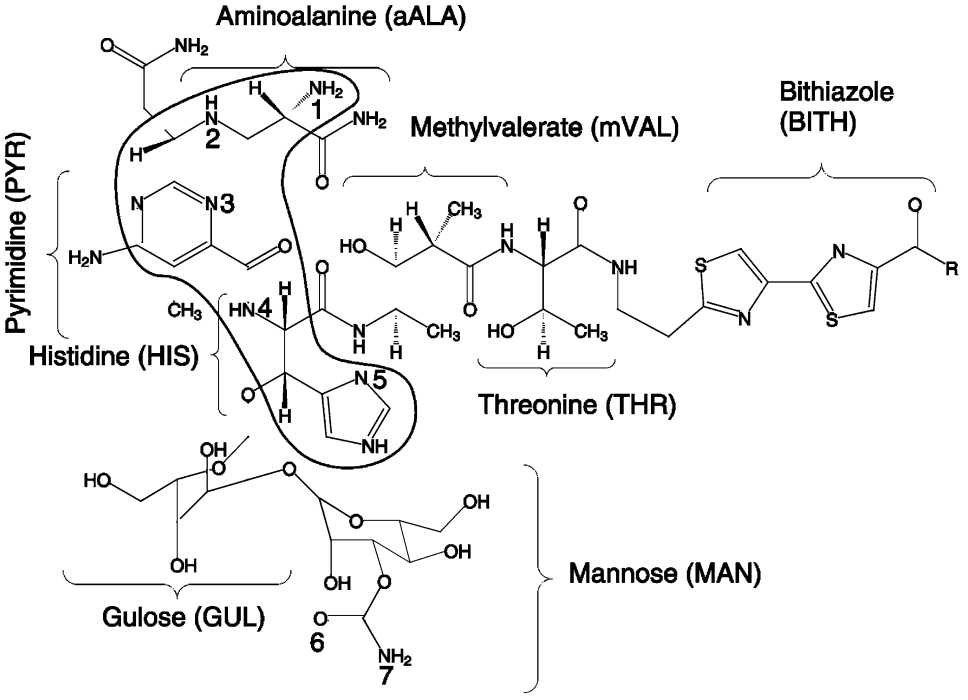

Bleomycin A_2 R = -NH$(CH_2)_3S^+(CH_2)_3$

B_2 R = -NH$(CH_2)_4$NHC(NH)(NH_2)

Peplomycin R = -NH$(CH_2)_3$NHCH(CH_3)Ph

Fig. 1 The structure of bleomycin A_2, B_2, and pepleomycin. The *numbers 1–7* indicate the possible coordination sites to the metal. The *loop* shows the PMAH ligand (2-{[*N*-(aminoethyl)amino] methyl}-4-{*N*-[2-(4-imidazolyl) ethyl]carbamoyl}-5-bromopyrimidine) [5]

deed present, whether it is endo- or exogenous. The exact coordination of the ligand has thus been a matter of dispute for several years. Most of the knowledge available on the structure of various metallo-BLM complexes in solution is derived from spectroscopic data [9, 10] and studies combining multinuclear NMR experiments and molecular dynamics simulations (MD) [11, 12]. Recently, Lehmann [12] proposed a very reasonable structure for Fe(II)BLM based on the results of such studies. The proposed model assumes that the complex has a six-coordinate structure with only endogenous ligands. The equatorial ligands to the metal center are the secondary amine of the β-aminoalanine (A″aALA – N2) segment, the pyrimidine (PYR – N3), the imidazole ring (HIS-I – N5), and the amide nitrogen (HIS-A – N4) of the β-hydroxyhistidine. The primary amine of the β-aminoalanine residue (A′aALA – N1) and the nitrogen atom from the carbamoyl group ($N_{carbamoyl}$ – N7) are the two axial ligands. This model is in agreement with other experimental work [10], where spectroscopic methods like optical absorption, circular dichroism, and magnetic circular dichroism were applied to determine the structure of Fe(II)BLM, except that the oxygen atom in the carbamoyl group ($O_{carbamoyl}$ – O6) is proposed as the sixth ligand. Therefore it is still unclear whether the nitrogen or the oxygen atom from the carbamoyl group is the second axial ligand.

The main goal of the present study is to solve the issue of the second axial ligand and to determine the structure of the Fe(II)BLM complex using density functional theory (DFT) calculations. We should emphasize that the coordination sphere of the iron atom depends crucially on the total spin of the complex. This important electronic contribution should be taken into account when using a force field method, e.g. as has been recently done for Cu(II) complexes by adding a ligand field contribution to the potential [13]. The model investigated here by first principles DFT is a realistic and comprehensive model of Fe(II)BLM, thus allowing us to check the limitations of previous studies on simplified models. Furthermore, we investigate the influence of protonation of the histidine amide nitrogen on the geometry of the complex. This aspect is important in the context of the long dispute over the inclusion of the amide nitrogen in the coordination sphere of the Fe(II)BLM complex. The protonation state seems to be highly dependent on pH: the ^{1}H NMR experiment by Oppenheimer et al. [14] at pH 6.4 provided evidence for a protonated state of the histidine amide and thus excluded it as a ligand. However, another NMR experiment by Akkerman et al. [15] at pH 7.0 showed that the histidine amide is deprotonated and bonded to the metal center under these conditions.

In the next section we describe in detail the models used for our studies and the computational method. In the third section we present our results and discuss them in comparison with available experimental data. The final section is devoted to conclusions.

Materials and methods

Computational details

Figure 1 shows a schematic structure of a metal-free BLM ligand. We can distinguish two parts: a main part, which is isostructural for the whole bleomycin family, and a long tail, which varies only in the terminal substituent denoted by "R". The main part is the metal bonding domain while the bithiazole tail is responsible for DNA docking [3]. We have investigated a model (Fig. 2) where only the bithiazole tail has been excluded, since it is most likely irrelevant to the coordination environment of the metal domain of the complex. Thus, our model provides a realistic description which can be used to develop insight into the geometrical and electronic structure of the Fe(II)BLM complex.

The starting structure was based on Co(II)BLM, generated from an NMR experiment [11], with the corresponding Co(II)-to-Fe(II) substitution of the metal center. Figure 3 shows the models used for this investigation. In Fig. 3a we show the six-coordinated complex with all endogenous ligands. Throughout the paper we define complex **A** as the model including in the coordination sphere the oxygen atom from the carbamoyl group. We call complex **B** the model obtained from complex **A** by rotation of the carbamoyl group in such a way that the nitrogen atom becomes the sixth ligand. Since we are interested in the influence of the protonation of BLM on the geometry of the complex, we have considered also the complexes **AH** and **BH** generated from complexes **A** and **B**, respectively, by protonation of the histidine amide nitrogen (N4). The index H indicates the protonated amide nitrogen (N4H).

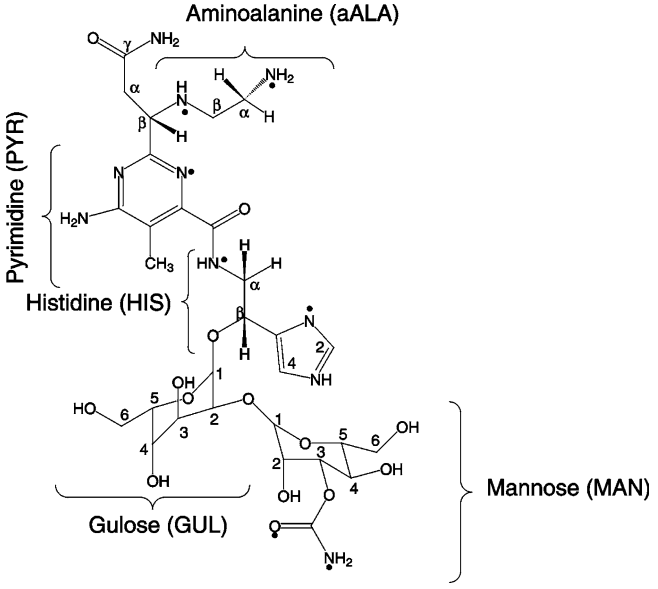

Fig. 2 Model of the BLM metal bonding domain used in this study. Some of the atoms are indicated with numbers and Greek letters following the same notation as in [34], for a direct comparison

In order to check the importance of the explicit inclusion of the original sixth ligand, we have also performed calculations on simpler models where the sugar moiety is replaced by either an ammonia molecule (complex **C**, Fig. 3b) or a water molecule (complex **D**, Fig. 3c). In this way we were able to check whether it is possible to answer the question about the second axial ligand based only on simplified models.

The DFT calculations were performed using the B3LYP functional, which was shown to predict the correct spin state for a number of different iron complexes [16, 17]. We used the effective core potential basis set LanL2DZ [18, 19] for the iron atom and the 6-31G basis set for the other atoms as implemented in the program GAUSSIAN98 [20]. This choice of the basis set is supported by the results of test calculations performed

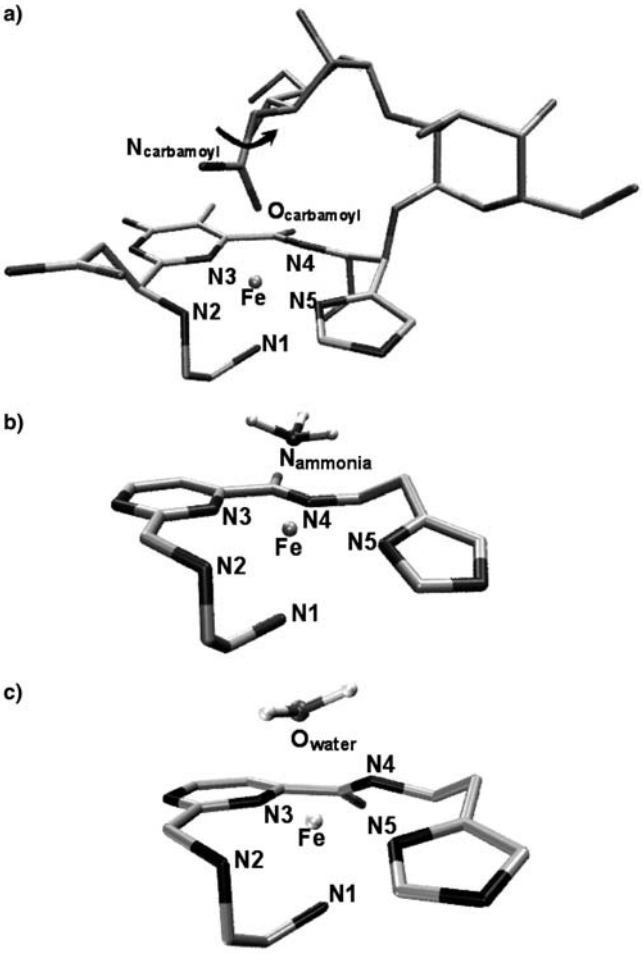

Fig. 3a–c Models of the metal coordination center domain of Fe(II)BLM with different axial ligands. (**a**) The oxygen atom from the carbamoyl group (complexes **A** and **AH**) and the nitrogen atom from carbamoyl group (complexes **B** and **BH**). Index H in **AH** and **BH** indicates the protonated amide nitrogen (N4H). Complexes **B** and **BH** were created by rotating the carbamoyl group via the torsion angle pointing in the picture. (**b**) The nitrogen atom from the ammonia molecule replacing the disaccharide moiety (complex **C**, see text). (**c**) The oxygen atom from the water molecule replacing the disaccharide moiety (complex **D**, see text) The hydrogen atoms have been omitted for simplicity

by Lehnert et al. [21] on similar model systems. Their conclusion is that the effective core potential basis set LanL2DZ is good enough to describe the geometry of ABLM and that a triple-ζ all-electron basis set gives a comparable description.

When comparing our results with structural information derived by NMR data in solution, one should take into account that we are neglecting solvent effects in our model. Although we can expect small changes in the geometrical parameters due to the solvent, we think that our conclusions on the coordination shell will not be affected. Indeed, it is now established in the literature that solvent molecules are not participating in the coordination sphere of the Fe(II)BLM complex [12, 22].

Results and discussion

For each system under consideration, full geometry optimizations assuming low, intermediate, and high spin states have been carried out. The final geometric parameters and electronic energies corresponding to singlet, triplet, and quintet states are summarized in Table 1 and Table 2 for protonated and deprotonated complexes, respectively. Complex **AH** was found to have the lowest energy in its quintet electronic state and this energy is taken as the reference energy for other spin states of complexes **AH** and **BH**. The same spin order is observed for deprotonated models and the energy of complex **A** in its quintet electronic state is taken as the reference energy for other spin states of complexes **A** and **B**. Our investigation shows that the geometry of the drug complex is highly dependent on the environment of the iron ion and on its spin state.

Complexes **A** and **AH**

For complexes **A** and **AH** the Fe–$O_{carbamoyl}$ distance changes as a function of the spin state, reaching a maximum value for $S=1$ (see Tables 1 and 2). In the complex **A**, this value is equal to 3.26 Å for $S=1$, indicating that the bond is broken. For $S=2$ the Fe–$O_{carbamoyl}$ bond is again present, with a length of 2.29 Å. Generally, the bond length between the iron center and its axial ligands ($O_{carbamoyl}$ and N1) in complex **A** are longer than in complex **AH** for each spin state (see Tables 1 and 2). This can be interpreted as a consequence of the deprotonation of the equatorial nitrogen donor ligand (N4) and the related shortening of the Fe–N4 bond length. It is known from ligand field theory that strong equatorial ligands cause a tetragonal distortion, which corresponds to an extension along the z-axis and compression on the x- and y-axes with a stabilizing effect on the d_{z^2} orbital. A natural bond orbital analysis shows that the d_{z^2} orbital is already lower in energy than the $d_{x^2}-d_{y^2}$ orbital for the protonated complex. Deprotonation of the amide nitrogen (N4) causes further lowering of the energy of the d_{z^2} orbital.

As the spin increases, each metal–equatorial ligand bond length generally increases and, in the particular case of N4 (complex **AH**), the distance increases up to 2.59 Å, while the average for the other equatorial ligands is 2.2 Å. Although this distance seems long, one can find structures in the Cambridge Structural Database of iron(II) complexes where the distances between iron(II) and its nitrogen donor are 2.50 Å [23], 2.54 Å [24], and even 2.65 Å [25]. Furthermore, the analysis of the HOMO orbital for β electrons (see Fig. S1 in the Supplementary material) shows that some weak bonding interaction is present between these two atoms, as indicated by overlap between the d_{z^2} orbital on iron and the lone pair on the N4 nitrogen atom. The same bond in complex **A** is less sensitive to a change in the spin (see Table 1). These results explain why it has been difficult to establish which atoms participate in the iron coordination shell. Hilbers and co-workers [15, 26] have proposed that BLM binds the metal through positions N2, N3, N4, N5, and N7, while Oppenheimer et al. [14] proposed N1, N2, N3, N5, and N7, thus excluding the N4 atom. These two studies used different experimental

Table 1 Relative energies and optimized geometric parameters for complexes **AH** and **BH**. All distances are in Å and angles in degrees

	Complex AH			Complex BH		
Total spin	0	1	2	0	1	2
ΔE(kcal/mol)[a]	11.48	15.12	0.00	36.50	31.41	16.92
Fe–X[b]	2.12	2.25	2.12	2.37	3.70	4.21
Fe–N1	2.04	2.20	2.20	2.05	2.23	2.18
Fe–N2	2.10	2.24	2.26	2.11	2.13	2.28
Fe–N3	1.93	1.94	2.14	1.91	1.92	2.07
Fe–N4	2.10	2.17	2.59	2.11	2.12	2.43
Fe–N5	2.02	2.01	2.22	2.04	2.04	2.16
X–Fe–N1	176.9	171.6	159.4	173.9	173.3	166.1
2–3–4–5	−1.6	−3.7	3.8	0.8	−3.2	−1.8

[a]For complexes **AH** and **BH** the reference energy is the ground quintet electronic state energy of the complex **AH**, which has the value $E_{ref}=-2968.9928$ a.u.
[b]X = $O_{carbamoyl}$, $N_{carbamoyl}$

Table 2 Relative energies and optimized geometry parameters of complexes **A**, **B**, **C**, and **D**. All distances are in Å and angles in degrees

	Complex **A**			Complex **B**			Complex **C**			Complex **D**		
Total spin	0	1	2	0	1	2	0	1	2	0	1	2
ΔE(kcal/mol)[a]	12.29	6.96	0.0	32.83	26.10	23.78	5.34	8.00	00.0	4.05	7.17	0.00
Fe–X[b]	2.17	3.26	2.29	2.29	3.93	4.02	2.07	2.28	2.26	2.07	2.32	2.22
Fe–N1	2.03	2.26	2.22	2.04	2.27	2.19	2.06	2.29	2.26	2.03	2.31	2.25
Fe–N2	2.16	2.13	2.40	2.14	2.15	2.30	2.17	2.35	2.48	2.15	2.25	2.42
Fe–N3	1.92	1.92	2.13	1.90	1.91	2.07	1.91	1.93	2.14	1.91	1.91	2.13
Fe–N4	1.97	1.94	2.09	1.98	1.94	2.03	1.99	1.99	2.07	1.99	1.97	2.06
Fe–N5	2.01	2.03	2.22	2.01	2.03	2.18	2.03	2.01	2.22	2.03	2.02	2.20
X–Fe–N1	170.3	126.2	140.8	176.8	168.4	166.2	179.3	165.6	161.9	177.9	157.8	155.3
2–3–4–5	7.0	9.4	14.7	5.9	7.0	9.4	5.5	5.3	4.5	−5.1	−5.6	−8.8

[a]For complexes **A** and **B** the reference energy is the ground quintet electronic state energy of the complex **A**, which has the value $E_{ref} = -2968.6627$ a.u. For complexes **C** and **D** the reference energies are the quintet electronic ground state energies, which have the values $E_{ref} = -1144.3408$ a.u. and $E_{ref} = -1164.1943$ a.u., respectively

[b]X = $O_{carbamoyl}$, $N_{carbamoyl}$, $N_{ammonia}$, O_{water} for complex **A**, **B**, **C**, **D**, respectively

conditions, including a different pH (pH 7.0 and 6.4, respectively). Our study clearly demonstrates that the problem of the ligand assignment can be related to the very weak bonding interaction between the N4 atom and the metal center when the pH is too low for the histidine amide to be deprotonated.

In the original model of the Co(II)BLM complex arising from NMR experiments combined with force field molecular dynamics simulation [11], the equatorial ligands are lying almost in the same plane. We observe a similar small distortion from planarity only for complex **AH** (see the 2–3–4–5 dihedral angle in Table 1). The largest distortion is observed for the deprotonated complex **A** in its quintet ground state, with a dihedral angle N2–N3–N4–N5 of 14.7°. The smallest distortion occurs for $S = 0$ (see Tables 1 and 2). Thus we conclude that the degree of distortion is highly dependent on the spin state of the complexes.

We also observe a large change in the valence angle of $O_{carbamoyl}$–Fe–N1 for different spin states (Tables 1 and 2). For complex **A**, the angle changes from 170.3° for $S = 0$ to 140.8° for $S = 2$. This angle distortion, together with the distortion from planarity discussed above, brings the complex into a highly distorted octahedral geometry. Because of these modifications, the Fe–$O_{carbamoyl}$ bond becomes weaker and more susceptible to exchange with an oxygen molecule to produce the Fe(II)O_2BLM complex. This complex then accepts an additional electron to form the activated BLM species. In previously proposed models for activated bleomycin based on force field methods [11, 27], the Fe–N1 bond was not present and the oxygen molecule entered the coordination sphere from the β-aminoalanine site. However, the crystal structure for copper-BLM [28] and some NMR studies for other metallo-BLM [29] suggest a different structure, in agreement with our results. Our results strongly support the picture in which the atoms N1, N2, N3, N4, and N5 remain in the coordination sphere of the metal center and the flexible sugar moiety drifts away, making space for an exogenous ligand.

Complexes **B** and **BH**

Complex **BH** also has the lowest energy for total spin $S = 2$, but this energy is still higher than the energy of complex **AH** for all spin states and, particularly, it is about 17 kcal/mol higher than the reference energy (the ground state of complex **AH** for $S = 2$). For complex **BH** the length of the Fe–$N_{carbamoyl}$ bond also increases with increasing total spin (see Table 1). Specifically, for $S = 2$ the distance becomes 4.21 Å, from which we can conclude that the $N_{carbamoyl}$ atom moves out of the coordination sphere of the iron atom. We notice that the breaking of the Fe–$N_{carbamoyl}$ bond also occurs in the **B** complex with the anionic ligand. Therefore, the behavior of the Fe–$N_{carbamoyl}$ bond is not related to the specific protonation state of the ligand, but rather to steric interaction. For $S = 0$ the distance between the $O_{carbamoyl}$ atom and the Cγ atom from the pyrimidine residue (Cγ_{PYR}) is equal to 2.89 Å, while the sum of van der Waals radius of these atoms is equal to 3.10 Å. When the Fe–$N_{carbamoyl}$ distance increases, the $O_{carbamoyl}$–Cγ_{PYR} distance increases as well, minimizing in this way the steric interaction. However, the presence of the proton affects the Fe–N4 bond. In particular, for $S = 2$ the Fe–N4 distance changes from 2.43 Å in **BH** to 2.03 Å in the complex **B**. Interestingly, the geometries of complexes **A** and **B** are very similar for the lowest spin state $S = 0$, both having a six-fold coordination shell. It is only when we go to the high-spin state ($S = 2$, the experimentally observed one) that we see major changes in the coordination shell. This strong dependence of the final geometry on the spin state of the complexes is an important information that should be taken into account when describing these systems in terms of force field modeling [13].

Complexes **C** and **D**

We have also investigated simplified models using an ammonia molecule (complex **C**) and a water molecule

(complex **D**) to represent the nitrogen and the oxygen atoms of the carbamoyl group, respectively, to check the importance of the inclusion of the large sugar moiety explicitly in the model. We find that the quintet electronic spin state is the ground state for both complexes **C** and **D**, which is in agreement with the experimentally observed spin state for Fe(II)BLM complex. However, the differences between energies of the different spin states and the reference energies are only a few kcal/mol (see Table 2) and we cannot directly compare energies of complex **C** and **D**. Both complexes form a distorted octahedral geometry, providing no grounds to distinguish between them. The Fe–$N_{ammonia}$ bond length increases slightly with increasing spin (Table 2), but we have not observed the bond breaking that occurs when the actual sugar moiety is included in the model (see complex **B**). By comparing the ground state structures of complex **C** and **D**, we do not observe a large difference in the X–Fe–N1 covalent angle as was the case in the complexes **A** and **B**. These results suggest that simplified models are not appropriate for resolving the issue of the sixth ligand of the Fe(II)BLM complex. Moreover, they also indicate that the disaccharide moiety plays a very important role in the metal bonding domain of BLM, showing that performing DFT calculations with the more realistic model is crucial.

Comparison with experiment

A quintet electronic ground state for the Fe(II)BLM complex was established many years ago using EPR [30, 31] and Mössbauer spectroscopies [31, 32]. Our B3LYP-DFT calculation is able to reproduce this spin state correctly. This is important, since previous DFT calculations [33] could not reproduce the proper experimental spin state. In [33] the calculations were carried out using B3LYP functional, as we have done here, but on a simpler model of bleomycin with only a penta-donor ligand and with a double deprotonated ligand (the histidine amide N4 and the secondary amine of the β-aminoalanine N2). The concordance between the observed spin state and the one computed here emphasizes again the importance of using a realistic model including all six potential donor sites.

We wish now to compare our optimized geometries with the available NMR data. Table 3 summarizes the comparison between the iron–proton DFT-optimized distances for the **AH**, **A**, **BH**, and **B** complexes in their ground electronic state, with the Fe–H distances based on 2D NMR studies of the paramagnetic complex Fe(II)BLM [34]. The experimental iron–proton distances were obtained from relaxation times of the paramagnetically behaved protons. The calculated root mean square deviation (RMSD) between experimental and theoretical data is 0.8 Å for both protonated models and 0.6 Å and 0.5 Å for deprotonated complexes **A** and **B**, respectively. However, if we consider only the mannose sugar moiety, which is directly connected to the carbamoyl group, the calculated partial RMSD for complex **AH** is 0.8 Å while for **BH** it is equal to 1.2 Å. For their deprotonated analogues these values are 0.5 Å and 0.8 Å, respectively. This implies that the structures of complexes **AH** and **A** fit better the experimental data than complexes **BH** and **B**, with respect to the part of particular interest for the nature of the sixth ligand. Indeed, we find the smallest RMSD value for the deprotonated models corresponding to the experimental conditions (pH 6.7) in the NMR study. The deprotonation of the N4 equatorial ligand influences the position of the axial $O_{carbamoyl}$ ligand. The Fe–N4 distance decreases while at the same time the Fe–$O_{carbamoyl}$ distance increases (Tables 1 and 2). This results in a better fit to the experimental data. Furthermore, Loeb et al. [10] concluded from their experimental work that the Fe(II)BLM complex is six-coordinate with at least five endogenous ligands and the sixth ligand being either the $O_{carbamoyl}$ substituent of the mannose sugar or a solvent molecule in this axial position. Their study did not determine whether the $O_{carbamoyl}$ atom is directly coordinated to the metal or connected through H-bonding. Based on our results and the information from the experimental work of Lehmann [12], we can now say

Table 3 Comparison of our theoretical results and experimental Fe–H distances (Å) from NMR data

Assignments[a]	Experimental data[b]	$S=2$ complex		$S=2$ complex	
		A	AH	B	BH
aALA $C^{\alpha}H$	3.7	3.3	3.3	3.3	3.4
1/2 aALA $C^{\beta}H_2$	4.1	4.2	4.1	4.1	4.1
1/2 aALA $C^{\beta}H_2$	3.4	3.5	3.4	3.4	3.3
PYR $C^{\beta}H$	<3.1	4.1	3.9	3.9	3.7
1/2 PYR $C^{\alpha}H_2$	4.8	5.0	4.9	5.0	5.1
1/2 PYR $C^{\alpha}H_2$	4.6	4.0	3.7	5.0	5.0
HIS $C^{\alpha}H$	3.6	4.1	4.6	4.0	4.2
HIS $C^{\beta}H$	4.4	4.6	4.9	4.6	4.6
HIS C2H	<3.2	3.4	3.2	3.4	3.3
HIS C4H	5.0	5.4	5.5	5.3	5.4
GUL-1	5.5	4.9	5.6	5.8	6.2
GUL-2	6.8	6.8	7.1	7.2	7.8
GUL-3	7.0	7.5	7.3	6.8	7.6
GUL-4	7.4	8.2	8.1	7.0	7.7
GUL-5	5.4	6.7	6.7	5.6	6.2
GUL-6	7.4	8.3	8.6	7.7	8.0
GUL-6	7.4	8.5	8.9	8.3	8.8
MAN-1	7.1	7.0	7.2	7.7	8.4
MAN-4	7.5	7.0	5.8	7.4	7.4
MAN-5	5.8	5.0	5.0	6.3	6.8
MAN-6	7.7	7.3	7.3	8.8	9.1
MAN-6	7.8	7.5	7.5	9.0	9.3
Total RMSD[c]	–	0.6	0.8	0.5	0.8
Partial RMSD[d]	–	0.5	0.8	0.8	1.2

[a] Notation has been taken from [34] (see Fig. 2)
[b] Experimental data are from [34]
[c] RMSD (root mean square deviation) calculated with the formula: $\sqrt{\frac{\sum (D_{exp}-D_{theor})^2}{N}}$ where D_{exp} and D_{theor} are the proton–metal distances derived from NMR data and our model, respectively; N is the number of data points
[d] RMSD only for mannose sugar moiety ($N=5$)

that the $O_{carbamoyl}$ atom is directly connected to the iron center, though in a highly distorted octahedral configuration.

Our findings are also in agreement with very recent data on Fe(II)-bleomycin obtained by X-ray absorption near-edge structure spectroscopy [22]. In this work the best agreement between theoretical and experimental spectra is achieved for the bleomycin model complex with the primary amine and oxygen of the mannose sugar occupying the axial positions. They also observed that the coordination environment is characterized by serious distortions of the iron octahedron.

Conclusions

We have performed DFT calculations on an extensive model of the Fe(II)BLM complex based on available NMR data [11, 34]. By comparing the model complexes **A** and **B**, distinguished by having the oxygen or the nitrogen atom from the carbamoyl group as the sixth ligand, respectively, we can conclude that the oxygen atom is coordinated to the metal center. We find that complex **A**, besides being energetically more favorable, also gives a better fit to the experimental data [10, 11, 32, 34]. We observe that in complex **B** the carbamoyl group tends to move out of the coordination shell in the high-spin configuration, contrary to experimental evidence. We suggest that this behavior can be explained in terms of the steric hindrance of the carbamoyl oxygen with the pyrimidine Cγ. The energetically most stable complex **A** in the high-spin configuration shows a highly distorted octahedral conformation, with an angle between axial ligands of 140.8°. This fact should facilitate the exchange of the $O_{carbamoyl}$ ligand with the oxygen molecule during the formation of ABLM.

We have investigated the effect of a different protonation state of the histidine amide on the geometric structure of the Fe(II)BLM complex. We observe that deprotonation of that equatorial ligand mainly influences the Fe–N4 distance, which is very long in the high-spin configuration of complexes **AH** and **BH**. It also affects the positions of the axial ligands, e.g. the Fe–$O_{carbamoyl}$ distance increases from 2.12 Å in complex **AH** to 2.29 Å in complex **A**, resulting in a better fit to experimental NMR distance estimates. The protonation state has no effect on the energetic spin order of our model complexes, nor does it influence the behavior of the carbamoyl group in complexes **B** and **BH**.

The study carried out with the simplified models shows that they are not appropriate for resolving the issue of the sixth ligand of the Fe(II)BLM. The results also indicate that the disaccharide moiety plays a very important role in the final structure of the metal bonding domain of BLM, showing that the use of a more realistic model in our DFT calculations is crucial. We also underline the importance of a theoretical method which directly takes into account the total spin of the system. This work provides a good starting point for further studies of the reaction mechanism of ABLM with DNA within the hybrid quantum mechanics–molecular mechanics (QM/MM) approach, provided a realistic QM active site of the activated BLM complex is considered.

Acknowledgements We would like to acknowledge Evert Jan Baerends for stimulating discussions. We thank Andrew Murray for a critical reading of the manuscript. A.K. is thankful to Pawel Rodziewicz for his help on computational issues.

Reference

1. Huang LR, Xie Y, Lown JW (1996) Expert Opin Ther Patents 6:893–899
2. Burger RM (1998) Chem Rev 98:1153–1169
3. Burger RM (2000) Struct Bonding 97:287–303
4. Brown SJ, Hudson SE, Stephan DW, Mascharak PK (1989) Inorg Chem 28:468–477
5. Brown SJ, Mascharak PK, Stephan DW (1988) J Am Chem Soc 110:1996–1997
6. Tan JD, Hudson SE, Brown SJ, Olmstead MM, Mascharak PK (1992) J Am Chem Soc 114:3841–3853
7. Kurosaki H, Hayashi K, Ishikawa Y, Goto M (1995) Chem Lett 691–692
8. Brown SJ, Olmstead MM, Mascharak PK (1990) Inorg Chem 29:3229–3234
9. Loeb KE, Zaleski JM, Westre TE, Guajardo RJ, Mascharak PK, Hedman B, Hodgson KO, Solomon EI (1995) J Am Chem Soc 117:4545–4561
10. Loeb KE, Zaleski JM, Hess CD, Hecht SM, Solomon EI (1998) J Am Chem Soc 120:1249–1259
11. Lehmann TE, Serrano ML, Que L (2000) Biochemistry 39:3886–3898
12. Lehmann TE (2002) J Biol Inorg Chem 7:305–312
13. Piquemal JP, Williams-Hubbard B, Fey N, Deeth RJ, Gresh N, Giessner-Prettre C (2003) J Comput Chem 24:1963–1970
14. Oppenheimer N, Rodriguez L, Hecht S (1979) Proc Natl Acad Sci USA 76:5616–5620
15. Akkerman MAJ, Neijman E, Wijmenga SS, Hilbers CW, Bermel W (1990) J Am Chem Soc 112:7462–7474
16. Fouqueau A, Mer S, Casida ME, Daku LML, Hauser A, Mineva T, Neese F (2004) J Chem Phys 120:9473–9486
17. Swart M, Groenhof AR, Ehlers AW, Lammertsma K (2004) J Phys Chem A 108:5479–5483
18. Hay PJ, Wadt WR (1985) J Chem Phys 82:270–283
19. Dunning TH Jr, Hay PJ (1976) Modern Theor Chem 3:1-28
20. Frisch MJ, Trucks GW, Schlegel HB, Scuseria GE, Robb MA, Cheeseman JR, Zakrzewski VG, Montgomery JA Jr, Stratmann RE, Burant JC, Dapprich S, Millam JM, Daniels AD, Kudin KN, Strain MC, Farkas Ö, Tomasi J, Barone V, Cossi M, Cammi R, Mennucci B, Pomelli C, Adamo C, Clifford S, Ochterski J, Petersson GA, Ayala PY, Cui Q, Morokuma K, Salvador P, Dannenberg JJ, Malick DK, Rabuck AD, Raghavachari K, Foresman JB, Cioslowski J, Ortiz JV, Baboul AG, Stefanov BB, Liu G, Liashenko A, Piskorz P, Komáromi I, Gomperts R, Martin RL, Fox DJ, Keith T, Al-Laham MA, Peng CY, Nanayakkara A, Challacombe M, Gill PMW, Johnson B, Chen W, Wong MW, Andres JL, Gonzalez C, Head-Gordon M, Replogle ES, Pople JA (1998) Gaussian98. Gaussian, Pittsburgh, Pa., USA
21. Lehnert N, Neese F, Ho RYN, Que L, Solomon EI (2002) J Am Chem Soc 124:10810–10822
22. Smolentsev G, Soldatov AV, Wasinger EC, Solomon EI (2004) Inorg Chem 43:1825–1827
23. Morgenstern-Badarau I, Lambert F, Philippe Renault J, Cesario M, Marechal J-D, Maseras F (2000) Inorg Chim Acta 297:338–350
24. Lonnon DG, Craig DC, Colbran SB (2002) Inorg Chem Commun 5:958–962

25. Sacconi L, Vaira MD (1978) Inorg Chem 17:810–815
26. Akkerman MAJ, Haasnoot CAG, Pandit UK, Hilbers CW (1988) Magn Reson Chem 26:793–802
27. Fedeles F, Zimmer M (2001) Inorg Chem 40:1557–1561
28. Sugiyama M, Kumagai T, Hayashida M, Maruyama M, Matoba Y (2002) J Biol Chem 277:2311–2320
29. Zhao CQ, Xia CW, Mao QK, Forsterling H, DeRose E, Antholine WE, Subczynski WK, Petering DH (2002) J Inorg Biochem 91:259–268
30. Burger RM, Peisach J, Band Horwitz S (1981) J Biol Chem 256:11636–11644
31. Peisach J, Burger RM, Band Horwitz S, Kent TA, Munck E (1983) Inorg Chim Acta 79:33
32. Burger RM, Kent TA, Band Horwitz S, Munck E, Peisach J (1983) J Biol Chem 258:1559–1564
33. Freindorf M, Kozlowski PM (2001) J Phys Chem A 105:7267–7272
34. Lehmann TE, Ming LJ, Rosen ME, Que L (1997) Biochemistry 36:2807–2816